Investigation of reinforced concrete members with bond deterioration under tensile load

◉A.I. Quadri ✉

Civil Engineering Department, Yokohama National University, (Yokohama, Japan)
✉: aiquadri@futa.edu.ng

ABSTRACT: Bond deterioration in reinforced concrete (RC) structures is frequently caused by aging, environmental factors, overloading, or poor design. This deterioration may cause the structure to lose its aesthetic, and eventually collapse. The behavior of structures that exhibit bond deterioration is poorly understood and inadequately maintained. The response of RC structures exhibiting bond loss under tension load is presented in this paper. In order to comprehend the impact of bond loss in RC composite, the RC system was first built for a pullout. It was then expanded to the nib corner of RC dapped end beams. Additionally, the system was analytically examined using 3-dimensional FEmodel. The bond loss created a weak zone with internal cracks parallel to the bar's axis. The nib section separated from the full depth of the dapped end, while the hanger reinforcement resisted the diagonal tension cracks. The dapped section must therefore be given more consideration during monitoring and maintenance.

KEY WORDS: Bond deterioration; Cracks; Dapped end beams; FEM analysis; Pull out.

RESUMEN: *Investigación de elementos de hormigón armado con pérdida de adherencia bajo carga de tracción.* Frecuentemente, la pérdida de adherencia en las estructuras de hormigón armado (RC) está causada por el envejecimiento, factores ambientales, sobrecarga o diseño deficiente. Este deterioro puede hacer que la estructura pierda su estética y, finalmente, colapse. El comportamiento de las estructuras que exhiben deterioro de la adherencia es poco conocido y mal entendido. En este documento se presenta la respuesta de las estructuras RC que exhiben pérdida de adherencia bajo carga de tensión. Con el fin de comprender el impacto de la pérdida de adherencia en el compuesto RC, se construyó dicho sistema para ensayos "pullout" y, posteriormente, se expandió a la esquina de los extremos de las vigas entalladas de RC. Además, el sistema se examinó analíticamente utilizando FEmodel de 3 dimensiones. La pérdida de adherencia creó una zona débil con fisuras internas paralelas al eje de la barra. La sección de la punta se separó de toda la profundidad del extremo perforado, mientras que el refuerzo del gancho resistió las fisuras de tensión diagonal. Por lo tanto, la sección no entallada se debe tener más en cuenta durante el monitoreo y el mantenimiento.

PALABRAS CLAVE: Pérdida de adherencia; Fisuras; Vigas de extremo entalladas; Análisis FEM; Pull out.

1. INTRODUCTION

The resistance of surrounding concrete to reinforcing bar pullout is referred to as a bond in reinforced concrete (RC). A bond is required between concrete and reinforcing bars to achieve an adequate level of safety by permitting composite action of reinforcing bars and concrete and to manage structural behaviour while maintaining sufficient ductility. For several decades, efforts have been geared toward understanding the impact of bond resistance between these two composites. If the bond resistance is insufficient, reinforcing bar slippage damages the RC adhesion properties (1–4). Brittle failure can occur in RC members when the bond between the rebars and the concrete in the anchorage zones breaks suddenly under sustained loads. Significant damage can be caused by the rotation of joints due to the bond loss in RC resulting in a slip of reinforcement (1, 5). Steel corrosion in RC structures can also lead to bond loss and ultimately collapse under loading (6). Numerous articles have also been reported on the effect of deformation patterns and rib geometry on bond strength (7–13). Lutz and Gergely (14, 15) identified three important mechanisms for bond resistance in RC structures; "the chemical adhesive, friction, and the mechanical interaction between the deformed bar and the surrounding concrete". The resistance of reinforcement in concrete relies on the frictional bond, which provides resistance to loading, and further loading mobilizes mechanical action between the rebar lugs and the concrete. Mechanical interaction causes inclined bearing forces, which cause transverse tensile stresses and internal inclined splitting (bond) cracks along reinforcing bars, as shown in Figure 1 (8). Thus, an increase in conical crack width towards the concrete surface results in a loss of bond resistance in RC.
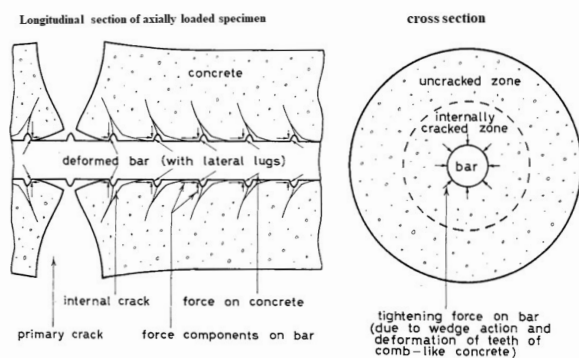

FIGURE 1. Internal cracks around reinforcing bar embedded in concrete (8).

1.1. Research outlook

A reassessment of the existing literature has shown considerable effort to understand the mechanism be-hind bond deformation of RC structures under loading. It has been proven that when a deformed bar is used as tensile reinforcement, the rebar ribs are bonded with the surrounding concrete. Concrete cracks around reinforcement are mainly connected to the durability effect and the binding mechanism problem between RC members. Cracks can lower the life expectancy of RC structures by allowing carbonation, chloride ion ingress, moisture migration, and oxygen to enter the reinforcement area (8, 16). Even while cracks accelerate corrosion, their effects are limited to the length of the bar parallel to the crack's width. As a result, concrete quality and cover thickness are critical criteria for preventing steel corrosion in concrete (17).

Therefore, this study considers the investigation of bond loss of RC by pullout reinforcement in cylindrical concrete to understand the essence of concrete cover in RC members under tension load with bond deterioration in lieu of corrosion and the residual bond interaction. PVC hollow pipes created the bond loss between the concrete and the reinforcing bar. Silicon gum was infused between the bar and the PVC hollow pipe to prevent free movement of the bar during testing. Moreover, structural members such as beam-column, corbel, dapped end beams (RCDEBs), and members with a sudden change in geometry often experience bond deterioration at the recess sections under loading due to the concentration of stresses at that point. To understand the behaviour of these structural members under loading, the author selected RCDEBs that exhibit tension damage at the dapped section. The bond loss was created at the nib of the dapped section of the beam and loaded monotonically till failure.

Furthermore, experimental evaluation and computational simulation of reinforced concrete structures are frequently used to analyze the nonlinear behaviour of concrete structures. Although the former yields accurate results, it can only explain occurrence under specific geometries, loading, boundary conditions, and cost (17). The latter involves creating computer models of reinforced concrete, which frequently has no boundaries. Numerical analysis is an alternative to the rigorous and expensive experimental study. The adaptability of the bond loss system in the experiment was then modelled in the Concrete Model of 3 Dimension (COM 3D) finite element software system to evaluate the efficiency of the software for large-scale adoption of structural members exhibiting bond deterioration.

1.2. Crack propagation around deformed bar under tension load

Tepfers (18) used finite element analysis to describe the radial components of bond forces balanced against tensile rings in concrete (FEA). Independent

of the rib face angle, the angle was 45° along a perimeter touching the ribs of reinforcing bars. The rib face angle influences the bond behaviour of bars with rib face angles (19). The bond behaviour changes when the rib face angle is less than 30°. Bond strength is reduced in bars with small rib spacing and height. Goto (8) tested the propagation of various cracks around tensile reinforcing bars. Internal cracks form around the reinforcing bars in concrete, as illustrated in Figure 2. The internal cracks are categorized as primary and secondary cracks. The former is generated at an angle perpendicular to the bar lug and propagated outward on the account of increasing stress; the latter is formed due to the slipping. Internal crack inclination and compressive force direction on bar ribs vary between 45° and 80°.
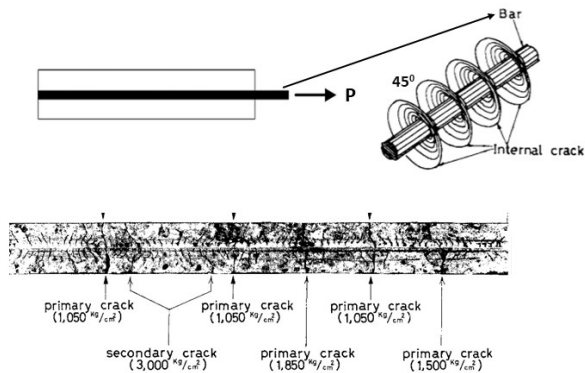

FIGURE 2. Failure response of concrete structures under tension.

1.3. Response of RCDEBs under loading

RCDEBs increase the lateral flexibility of structural support members, can also reduce the total height distance of precast concrete frameworks, and often has a lower self-weight due to a change in the cross-section of the reentrant portion (20, 21). They have also been used in precast bridge girder members. They have recessed ends supported by cantilevers, columns, corbels, or inverted T-beams (22). Nevertheless, RCDEBs are weakened at the reentrant corner because the flow of internal stresses is disrupted by the change in the cross sections, resulting in zones of non-uniform stress distribution near the reentrant corner and the nib (23). Due to the high bearing reaction and the alteration in geometry, the reentrant corner has a high-stress intensity. These discontinuities in a member are referred to as disturbed regions (D-regions) (24–26). The formation of diagonal tension cracks will reduce the strength of the full-depth part of the dapped end under the yielding of the hanger reinforcing bars, as shown in Figure 3. Mattock and Chan (27), and Aswin *et al.* (28) identified different cracks leading to failure of the RCDEBs. The failure includes; the diagonal tension cracks at the reentrant

corner, nib and undapped critical portion, flexural and axial tension at the extended end, and direct vertical shear between the nib and the undapped end. The shear strength performance of the RCDEBs depends on the nib-to-full depth ratio and spacing of the hanger bar close to the dapped end (29). Changes in nominal shear span and height of the nib will give different diagonal tension strength capacities of RCDEBs. Mohammed *et al.*, (30) evaluated the performance of RC and R-ECC DEB on the role of stirrups and the diagonal reinforcing bar, although the investigation was remarkable with an increase in failure load while there was a delayed in crack initiation, the reentrant portion lost its confining strength which resulted in damage at the tension zone. Due to anchorage deterioration and overloading, the failure of bridges with dapped ends has been rampant in the last decade. Failure of the De la Concorde bridge in Canada was reported in 2006 due to bond deterioration of the anchorage zone (31). The collapse of the Annone overpass in Italy was reported recently due to corrosion of prestressed tendons at the anchorage zone (32-34). Maintenance of the dapped section (anchorage zone) of RCDEBs in the bridge girder requires excellent effort due to this recess portions that sit on other structural members; water or eroded materials can amass on this part, which can hasten the deterioration of the beam by causing corrosion concern (17). It is thus necessary to understand the damage mode of the RCDEBs subjected to increasing monotonic load under bond deterioration to proffer strategies for monitoring and maintenance for practical engineering.
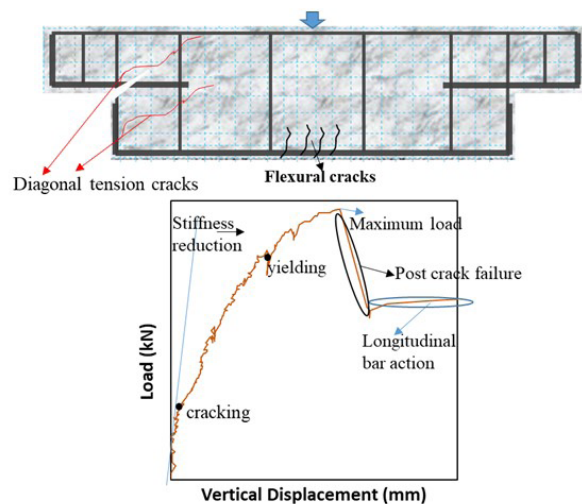

FIGURE 3. Failure response of RCDEB under increasing monotonic loading.

2. EXPERIMENTAL SETUP FOR PULLOUT TEST

A total of six (6) steel cylindrical molds with a diameter of 150 mm and height of 300 mm were set

up for the pullout tests. A hollow PVC plastic pipe with an inner diameter of 25 mm was used to simulate bond loss in place of corrosion. Two specimens were selected as control samples, while the bond loss was made in the other specimens either at the bottom or the middle of the specimens, as shown in Figure 4. 22 mm deformed bar was inserted inside the PVC pipe (40 mm deep) and bonded with silicon gum to prevent slipping of the bar inside the pipe, the bar protruded out of the cylinder mold by 20 mm held in position with a wooden plank, which covered the bottom face of the cylindrical mold for easy concrete casting. Steel strain gauges of 5 mm were mounted on the steel bar, and 60 mm strain gauges were also mounted on the concrete to measure the strain development during loading, as displayed in Figure 4. The position of the strain gauges has been confirmed during concrete compressive and steel tensile tests, as presented in Figure 8.

2.1. FEM model of the pullout test specimens

The FEM of the specimen was carried out with the aid of the COM 3D system, under the multi-fixed crack approach, COM3D focuses on the full model of the reinforcement inside the concrete material to form the RC mesh. The reinforcing bar in Figure 5 was modelled in one dimension with the yield stress of the bar. The mesh density was accounted for here to avoid the coarseness of the FEM mesh, which could lead to unreliable output during loading. The exact dimension in Figure 4 was considered for the analytical model of pullout specimen. The hollow PVC plastic pipe properties were inserted into the mesh at the vicinity of the rebar where necessary, with a bond interface applied between the mesh and the embedded reinforcing bars. When investigating the response of RC structure under loading, it is essential
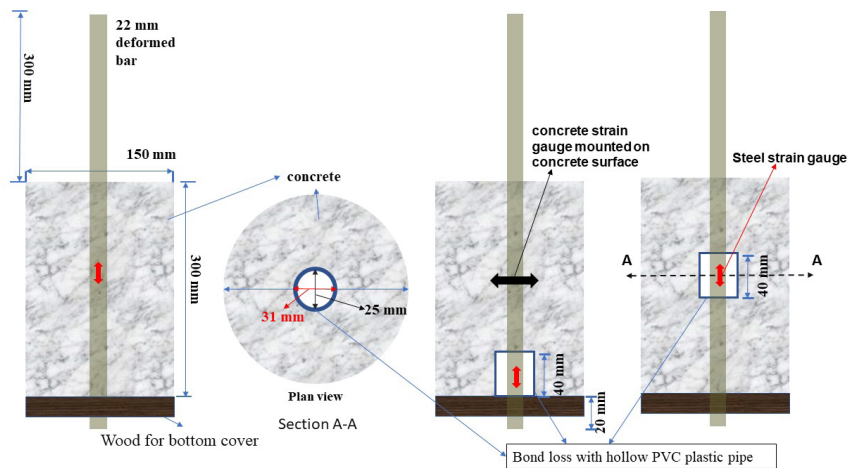

FIGURE 4. Specimen model for pull out test.
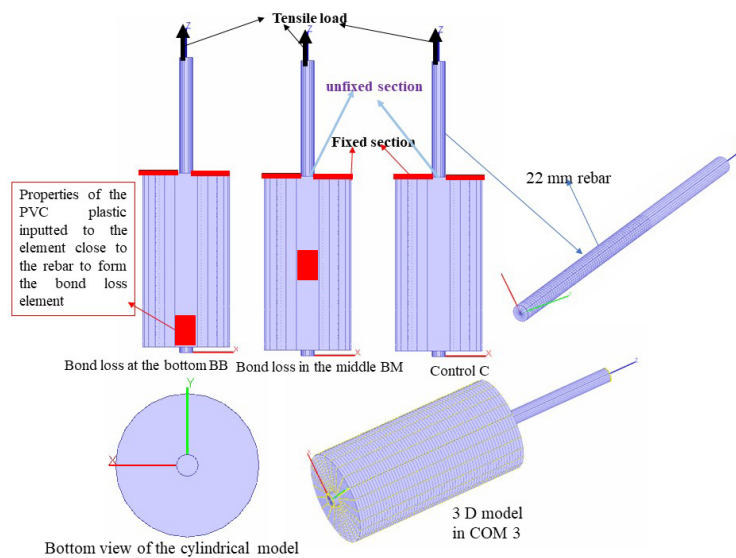

FIGURE 5. FEM model of the pull out.

to consider the bond interaction between the composites. COM3 permits the model of the bond interface between the composite to ensure adequate bonding. Figure 6 shows the bond interface element model used in place of steel and concrete properties under Mohr-Coulomb's frictional law (34). Table 1 shows some of the properties of concrete, steel PVC plastic materials and the interface element considered during the analysis of the bond loss.

Figure 7 is the constitutive model of RC considered under the active fixed crack approach, where the stresses generated from the RC are a simple summation of the concrete crack model and the embedded reinforcing bar. The combination of the tension softening-stiffening model normal to cracks, compression-tension model along cracks, and shear transfer along cracks is required to develop the stress-strain relationship of cracked concrete in the elastoplastic domain. Some governing equations have been presented under the active fixed crack approach (35, 36).

2.2. Casting and loading of pullout specimens

M35 concrete mix grade was designed to achieve a 28-day characteristic cylindrical compressive strength of 35 MPa. Ordinary Portland cement, fine aggregate, and coarse aggregate with a maximum aggregate size of 20 mm are the constituents of the concrete mix, as presented in Table 2. The water-cement ratio (w/c)
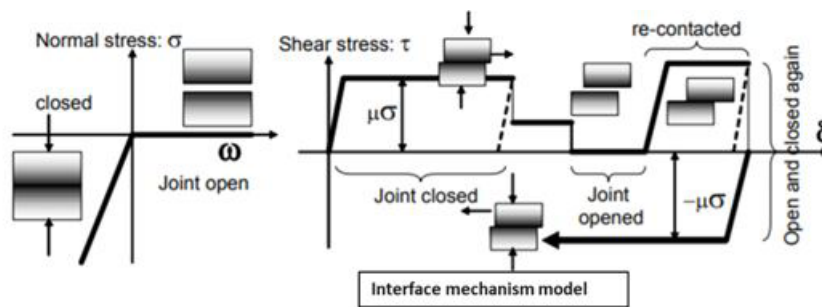

FIGURE 6. Interface element model (34).

TABLE 1. Material strength properties for analysis.

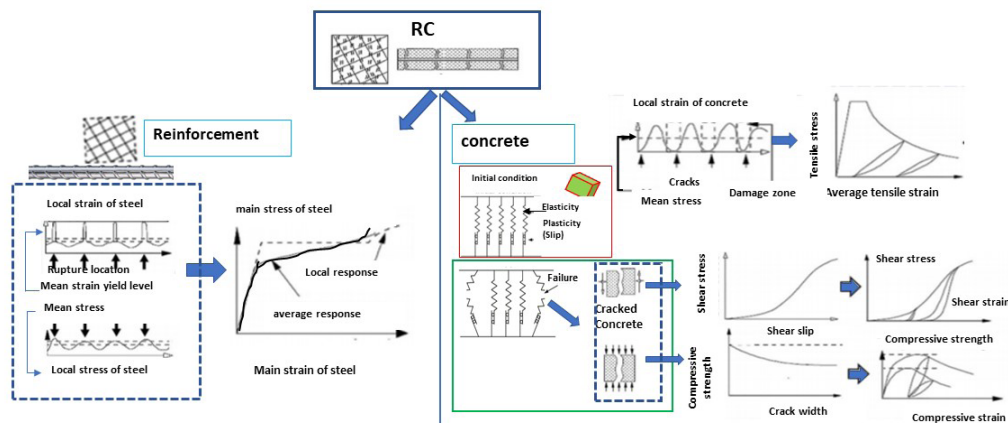| Material Property	Concrete (N/mm²)	Steel (N/mm²)	Plastic Material (N/mm²)	Interface element properties	
				Coulomb friction	
Initial stiffness	2.2×10^5	2.1×10^6	3.3×10^4	Shear stiffness	3×10^5
Poisson ratio	0.2	0.3	0.2	Normal stiffness	3×10^5
Unit weight	24	78.6	14.5	Friction coefficient	0.65
Tensile strength	2.48	-	51.7		

FIGURE 7. Constitutive model of reinforced concrete.

was 0.43, and the air-entraining water-reducing agent was 0.3% by weight of cement. In addition to the cast specimens, cylindrical sizes of 100 mm diameter and 200 mm height were cast to determine the concrete's compressive strength and split tensile strength. The slump and air entrainment test results are 110 mm and 1.75%, respectively. The tensile strength of the rein-forcing bars was determined in the laboratory using a universal testing machine with a capacity of 1000 kN. Figure 8 shows the plot of stress versus strain of the tensile test results of the 22 mm and 10 mm diameter bars and concrete compressive strength. The strains were captured with the strain gauges attached to the data logger machine. The test results made part of the input data in the analysis. The yield stress and ulti-mate strength of the 22 mm diameter bar are 410 MPa and 544 MPa, respectively, while the yield stress and ultimate strength of the 10 mm diameter bar are 500 MPa and 614 MPa, respectively.

Six specimens of the pull out tests were prepared in total (two for each series). Table 3 describes all the spec-imens, the compressive strength and splitting test for experimental investigation and analysis. The prepared pullout molds with the rebar centrally placed inside and the steel strain gauges affixed to the steel in Figure 9 were cast in three layers, each layer was compacted twenty-five times with a tamping rod, and the top sur-face smoothened. The binding wire was used to support the rebar at the upper part of the mold to achieve a per-sistent condition, while the lower part was guided with polystyrene material. The specimens were covered with a wet curing sheet and cured continuously for 7 days. After the seventh day, the cast specimens were demold-ed and wrapped in a wet curing sheet for the remaining 28 days, where water was constantly provided for cur-ing. Concrete strain gauges were attached to all the spec-imens in the transverse direction to measure the concrete strain development during loading.

A universal testing machine (UTM) of 1000 kN capacity was used for the pullout test, as shown in Figure 9 (right side). The pullout specimen was put into the machine such that the movable part of the machine held the unintegrated length of the deformed bar to pull it out of concrete during testing, while the static part held the concrete in position. A hollow base plate with a 50 mm centrally bore-hole was provided on top of the static part where the concrete sat, and the unintegrated length of the steel was passed through the hollow base plate and anchored on the movable part. Gypsum flakes were prepared to balance the concrete so that the applied load could be evenly dis-tributed during testing. The steel strain gauges and that of concrete were connected to the data logger to retrieve the strain response of the RC during the pullout. A displacement transducer (LVDT) was also mounted on the movable part to measure the amount of displacement up to the maximum load. The top surface of the concrete was fixed in the case of FEM loading of the pullout analysis, while the tensile load was applied at the tip of the steel (Figure 5). The bot-tom of the specimen was not supported to imitate the exact circumstances in the experiment.
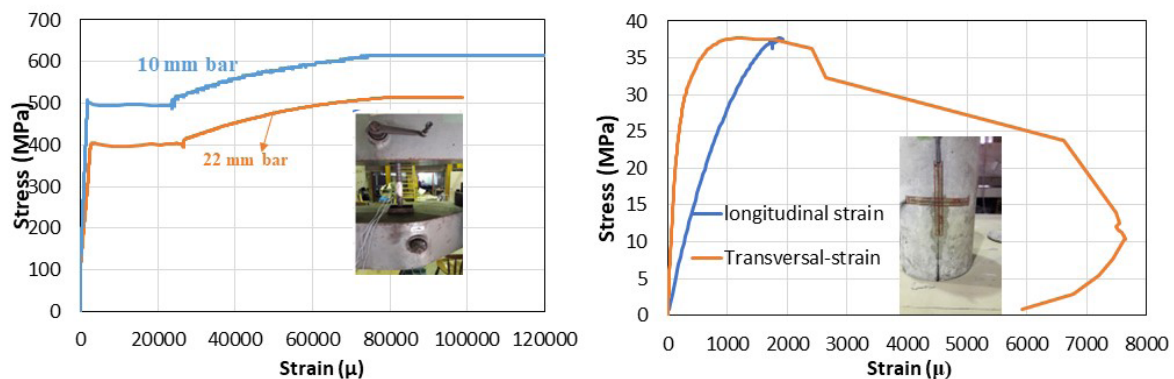

FIGURE 8. Strength test result of steel and concrete.

TABLE 2. Concrete mix proportion.

G_{max} (mm)	W/C	Unit weight (kg/m³)				
		W	C	S	G	AE
20	0.43	172	400	640	1160	1.2

G_{max}: Maximum size of coarse aggregate; W: water; C: cement, S: fine aggregate; G: coarse aggregate; AE: air-entrainment water-reducing agent.
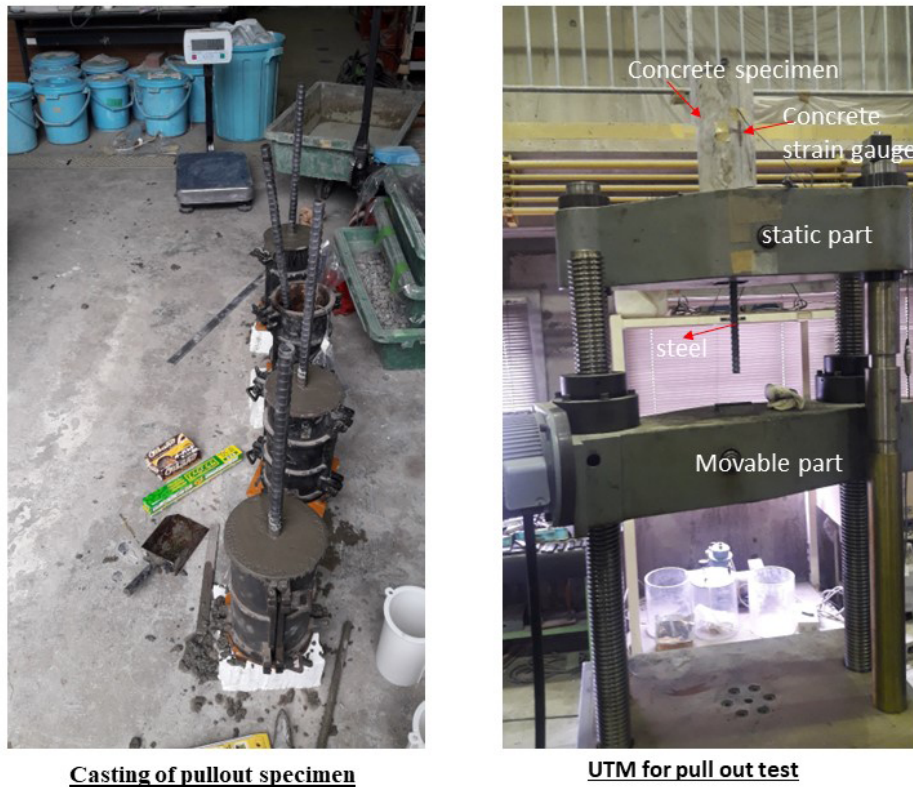
Casting of pullout specimen

UTM for pull out test

FIGURE 9. Formwork and load setup.

TABLE 3. Specimen description and concrete strength.

Specimen Pull out	Specimen description		Concrete strength (N/mm²)	
			compressive	splitting
Control	Control experiment 1	C1	42	2.5
	Control experiment 2	C2	38	2.5
	Control analysis	CA	42	2.7
Bond loss at bottom	experiment 1	BB1	42	2.7
	experiment 2	BB2	38	2.5
	Analysis	BBA	42	2.7
Bond loss at middle	experiment 1	BM1	42	2.7
	experiment 2	BM2	42	2.7
	Analysis	BMA	42	2.7

3. RESULTS AND DISCUSSION ON RESPONSE OF PULLOUT

Figure 10 illustrates the global damage of the pullout specimens during the experiment and the maximum principal strain of FEM analysis. In the case of the experiment, the nonlinearity of concrete manifested at relatively high steel stress, with concrete cracks parallel to the steel first detected in all specimens and extended in width. As the pullout force was raised, further cracks formed and propagated towards the concrete surface, generating a fan-blade shape in the bond loss specimens. Shortly after the mature cracks occurred, little internal

cracks appeared that could not be seen on the concrete surface. When the specimen was split, and the deformed bar was carefully removed, internal cracks running longitudinally along the bar where the PVC pipe did not cover and hairy-like cracks normal to the bar axis were observed.

The maximum principal strain of the pullout specimen under FEM analysis was evaluated and presented in Figure 10, it is considered that adhesion between the concrete and the steel had been lost at this point; this loss of adhesion appeared at the bar surface close to the first visible cracks. The damage mode is nearly the same as the experiment. Thus, internal cracks significantly impact the bond mechanism between the concrete and the steel. Observing the internal stress response, the concrete crack developed around the steel exhibits complex teeth in the direction of the closest cracks caused by compressive forces transferred from the bar ribs as steel tension is elevated.

3.1. Load versus displacement and strain response of the pullout specimens

The cracking load, load at failure and the deflection/slip of the pullout specimens for both experimental investigation and analysis are presented in Table 4. The load that generated the initial concrete cracks
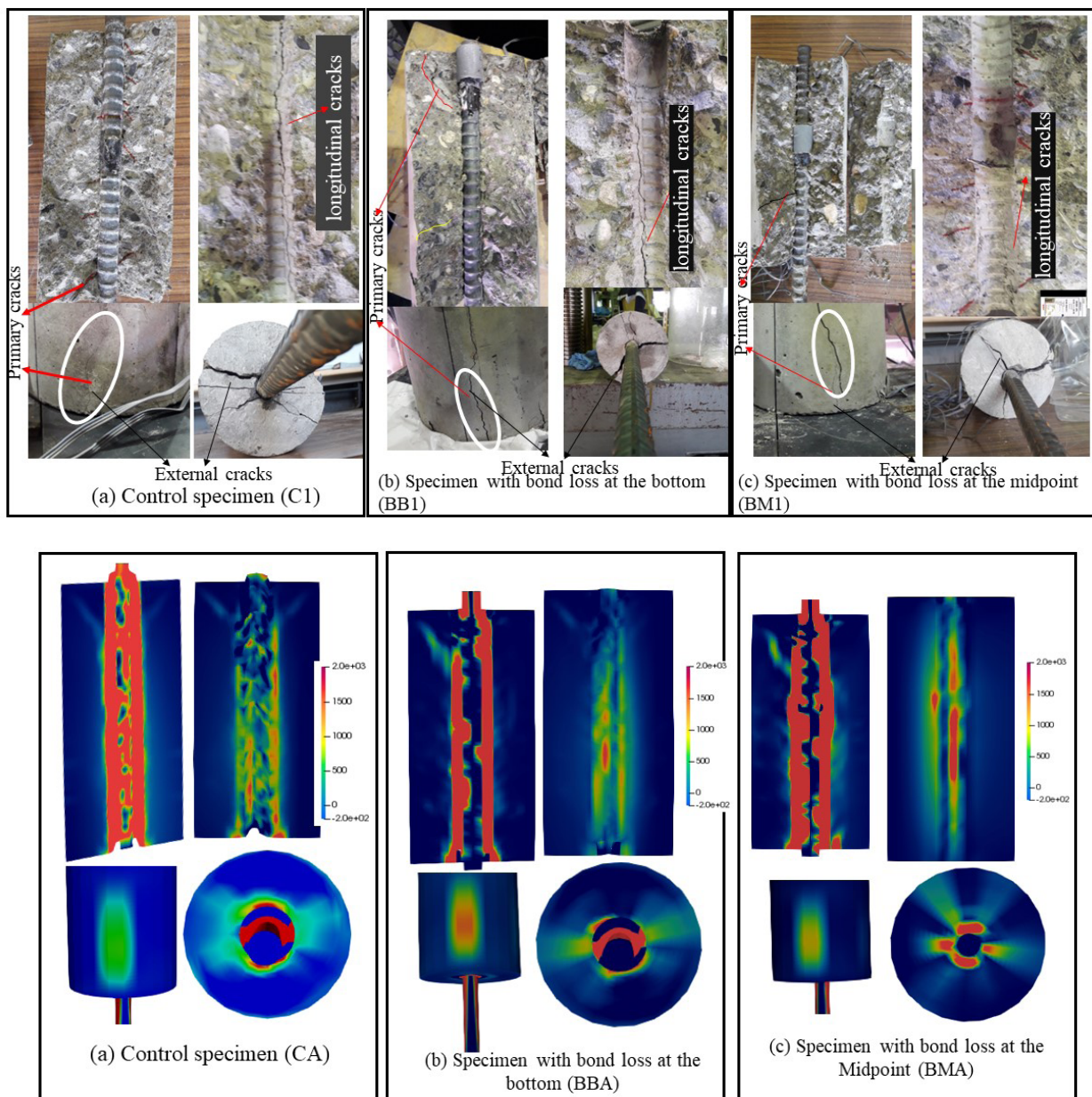

FIGURE 10. Global damage mode of experimental pullout specimens and Maximum principal strain of global damage of FEM.

was considered since it signified the emergence of RC nonlinearity. The equivalent displacement, δ_y, was also assessed. The ductility ratio, $^{\Delta_u}/_{\delta_y}$, defines the ratio of initial crack displacement to the failure load displacement (37). Generally, the pullout analysis revealed a significant increase in capacity with high stiffness and deformation over the experiment in each group except for C1, as shown in Figure 11. This could result from increased concrete compressive and splitting strength (see Table 3). There is a reduction in slip displacement when the bond loss is considered at the bottom since the concrete crack emerged from the weak bond zone. When comparing the failure capacity of the experimental specimen, C1 increases by 10% and 11% over BB1 and BM1, respectively, and 2% and 8% over the analyses of BMA and BBA. While the failure capacity of the control analysis CA is the same as that of the BMA, it increases by 6% over the BBA.

Figures 12 and 13 show the load versus strain generated from reinforcement and concrete. The strain was measured by strain gauges mounted on both the surface of the reinforcement and concrete in the case of the experiment. In contrast, the space average of the strains under the active crack approach of the most stressed portion of the specimen was examined in the case of the analysis investigation. Apparently, a linear-elastic relationship initially occurred before concrete cracking. The reinforcement strain moderately increased as soon as the micro-cracks was generated, and a further increase in load resulted in the nonlinearity of the RC. Although there is no yielding point of reinforcement in all the specimens up to the failure load, as presented in Figure 12 (at a yield value of 2000μ), concrete began to crack as soon as the tensile stress generated exceeded the tensile strength of concrete. The concrete strain of -200μ has fairly been exceeded as indicated in Figure 12, except in BB2, due to the detachment of the strain gauge during loading.

TABLE 4. Specimen's load and deflection.

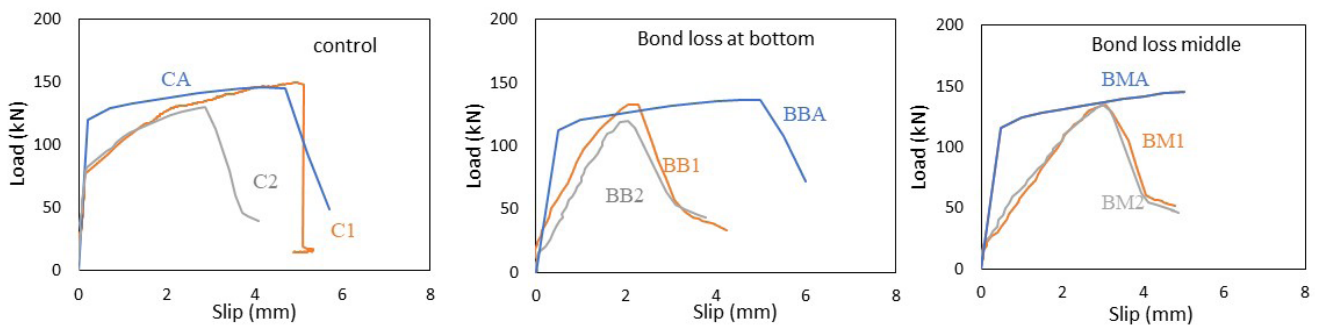| Specimen Pull out	Name	Loading and deflection (kN and mm)				
		at cracking	δ_y	at failure	Δ_u	Ductility ratio $\left(\Delta_u/\delta_y\right)$
Control	C1	61.28	0.1	148.01	5.1	51
	C2	55	0.1	130.21	2.9	29
	CA	79.15	0.15	145.12	4.7	31.33
Bond loss at bottom	BB1	25.62	0.1	132.96	2.3	23
	BB2	19.07	0.2	120.06	2.1	10.5
	BBA	43.43	0.2	136.39	5.0	25
Bond loss at middle	BM1	25.10	0.1	134.69	3.0	30
	BM2	25.22	0.1	134.72	3.0	30
	BMA	40.22	0.2	145.02	5.0	25

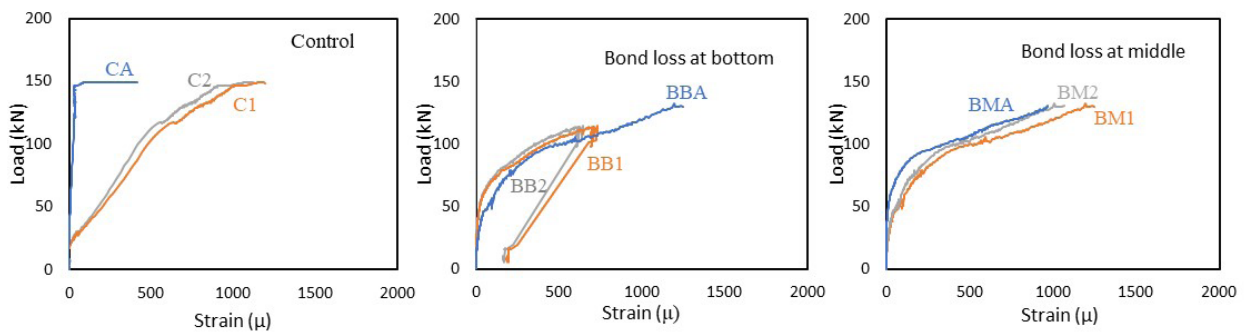FIGURE 11. Load versus slip response under pull out.

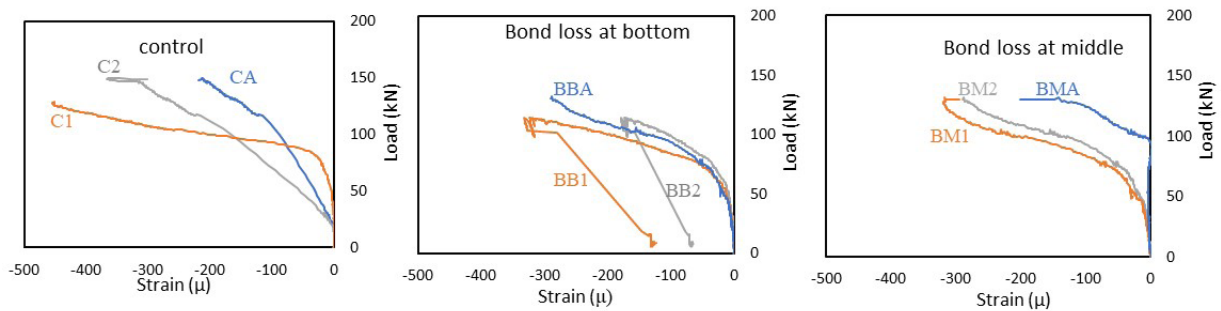**FIGURE 12.** Load versus strain of reinforcement.

FIGURE 13. Load versus strain of concrete.

4. INVESTIGTION OF BOND LOSS IN RCDEBS

4.1. Reinforcement detailing of RCDEB

The struts and Ties approach was adopted to model the reinforcing bars detailing the RCDEB. Figure 14 depicts the strut-and-Tie flow chart model as well as the specimen's reinforcement detailing. The chosen dimensions are 1600 mm × 200 mm × 400 mm in length, width, and depth. The dapped end's length, width, and depth are 300 mm × 200 mm × 200 mm. All stirrups were made of 10 mm diameter deformed bars with 150 mm centre-to-centre spacing close to the dapped portion and 210 mm centre-to-centre spacing in the middle. The nib longitudinal tensile and flexural bars were reinforced with 22 mm diameter reinforcing bars. Two series of RCDEBs specimens were considered, the control specimen and the bond loss specimen made with the PVC plastic hollow pipe was infused at the recessed corner, as shown in Figure 15. The same diameter of PVC pipe considered for the pullout specimen was used, with a length of 140 mm. steel strain gauges of 5 mm were mounted on both the stirrup bars close to the reentrant section and the longitudinal bar at the nib section, while 60 mm concrete strain gauges were mounted on the concrete.

4.1.2. FEM analysis of RCDEB

Figure 16 depicts the modelling of RCDEB using the COM 3D system, with the same dimension consid-ered for the experimental approach and the reinforcing bars detailing using the STM. To achieve slipping of the longitudinal nib reinforcement, the bond loss was modelled close to the dapped section using the plastic properties in Table 1 and the bond interface element model (see Figure 6). To achieve equilibrium, the simple support was made elastic. The author used discrete modelling of the reinforcing bar, which allows the reinforcing bars to be arranged inside the RCDEB model's elements. The discrete model is more stable during the analysis process because it resembles the exact arrangement in the experimental approach. In the nonlinear simulation of the RCDEB, the typical model comprises 4,288 elements and 7,234 nodes with elastic support designed as simply supported.

4.2. Casting of specimens and loading

Steel formwork was set up for RCDEB casting with plywood used to create the dapped-ends, detailed reinforcement was placed inside the formwork, and freshly prepared concrete was poured inside the formwork and vibrated with a vibrating machine to achieve workable concrete as shown in Figure 17 (left side). Four beams were cast, two for control and the others for bond loss, using PVC hollow pipe.

The RCDEB specimens were instrumented to obtain enough data recorded by the data logger, particularly at the dapped section where the bond loss occurred. The steel strains were measured with 5 mm
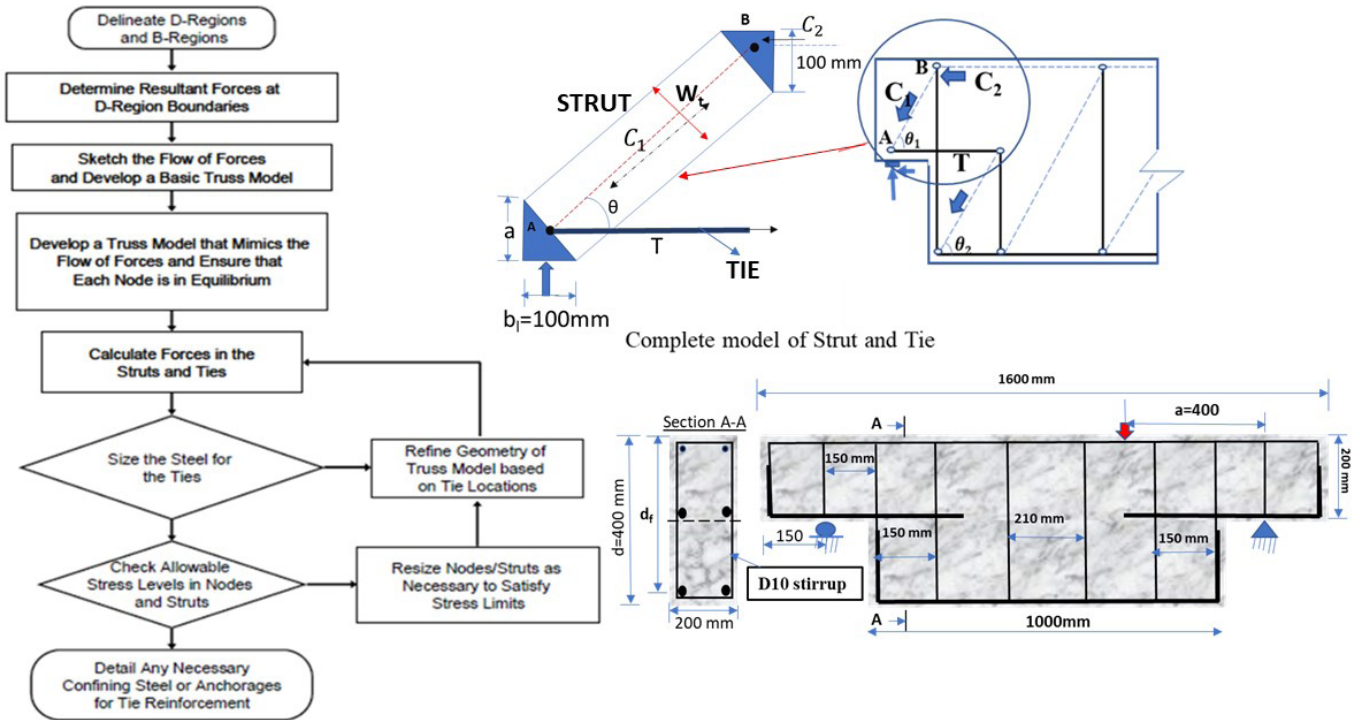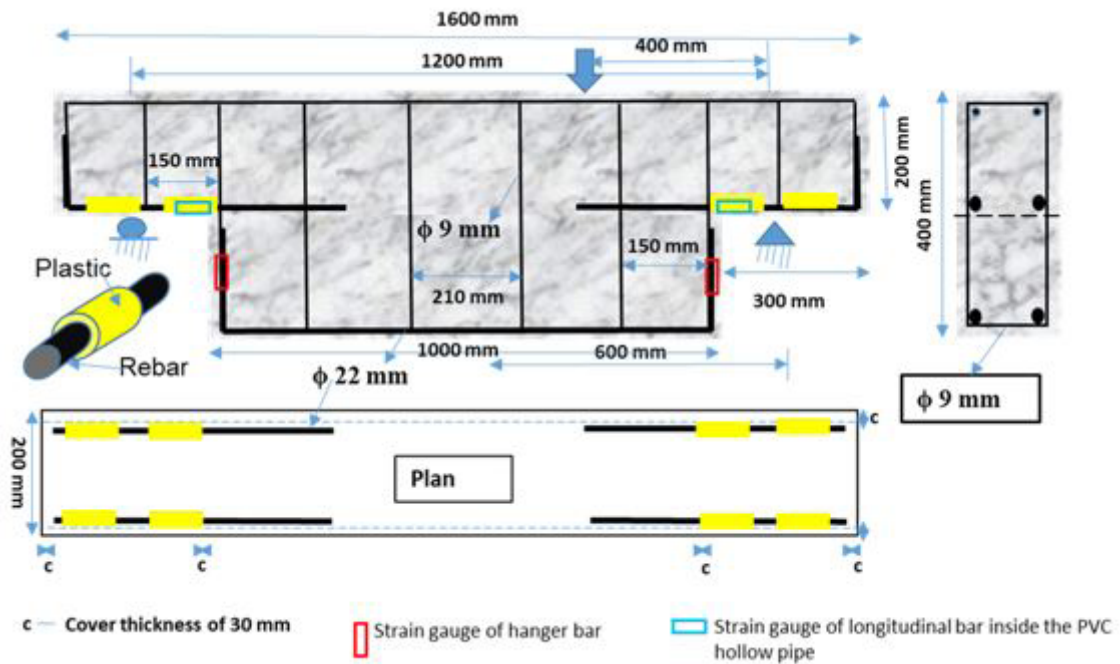
FIGURE 14. Struts and ties model of RCDEB.

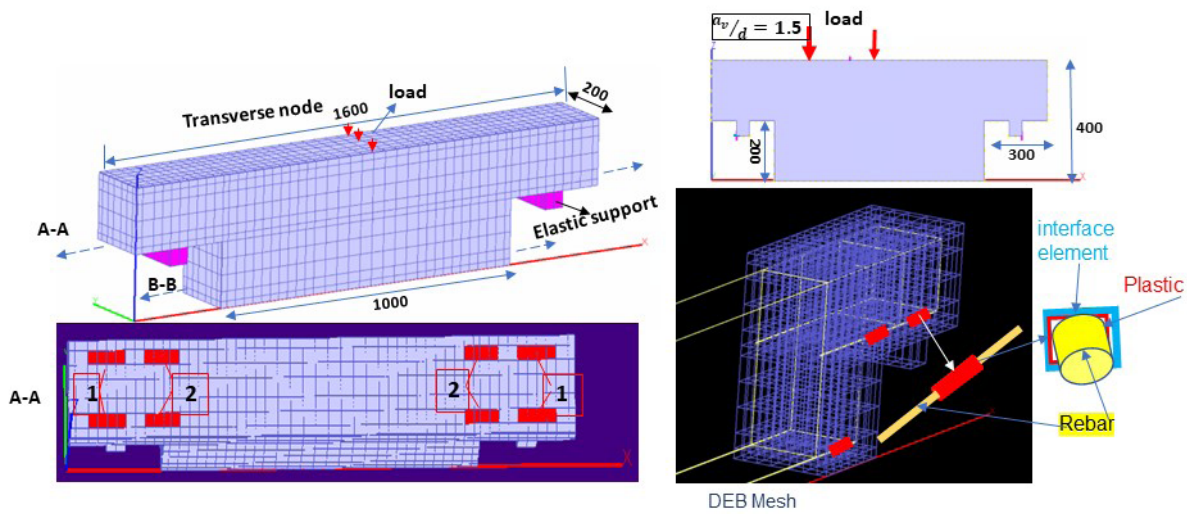**FIGURE 15.** Modelling of RCDEB with bond loss.

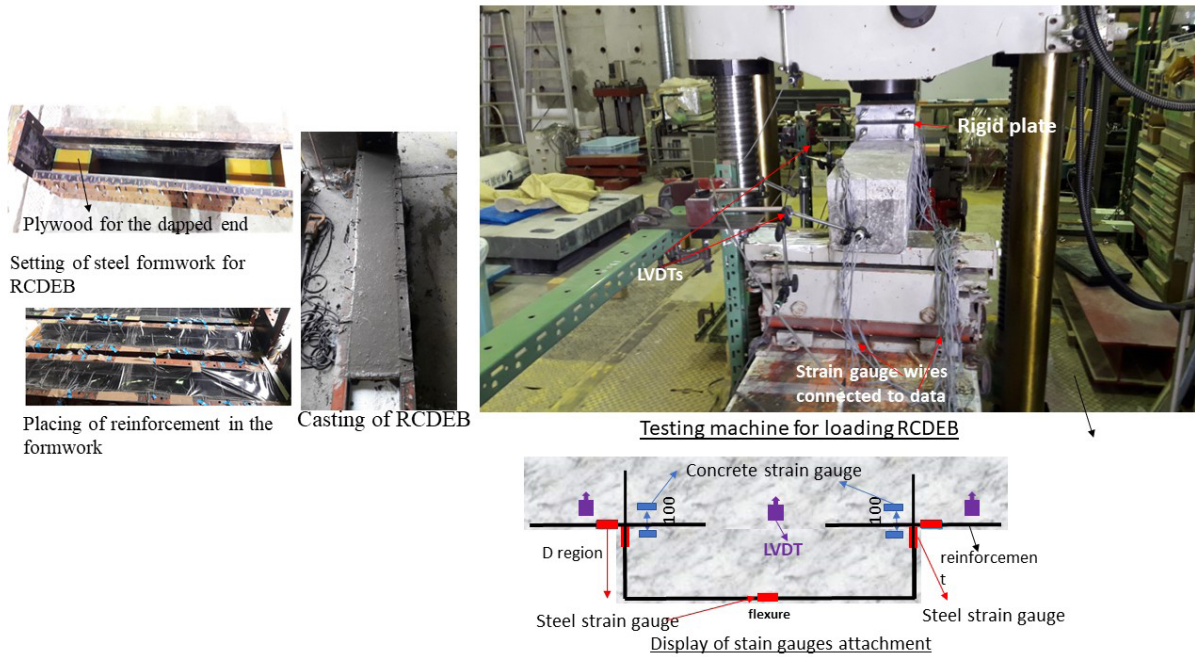**FIGURE 16.** RCDEB FEM analysis (all dimensions in mm).

FIGURE 17. Formwork and load setup.

electrical resistance steel strain gauges mounted to the longitudinal reinforcement at the nib and flexure zones. The strain gauges were also attached to the hanger reinforcement on the left and right sides of the beam to evaluate the strain values developed during loading. 60 mm concrete strain gauges were also attached to the concrete surface close to the dapped end. Three 25 mm capacity LVDTs were placed on the beam at the lower portion of the loading point and the top side of the supports to measure the vertical displacement of the beam. The test beams were subjected to three-point bending on a UTM with a capacity of 2000 kN in Figure 17 (right side), where the load was applied at a shear span to depth ratio (a/d) of 1.5

and the midpoint for the two series considered. A top steel rigid plate 200 mm × 200 mm was employed to transfer the load from the machine head to the beam. The load was applied in 5 kN increments till failure. In the case of the RCDEB FEM study, the incremental static load was applied at the transverse nodes, either at the midpoint or a/d, as the case may be (Figure 16).

4.3. Damage mode of RCDEB

Figures 18 and 19 show the damage patterns of RCDEB subjected to increasing monotonic load at a/d=1.5 and the midpoint. The first crack generally
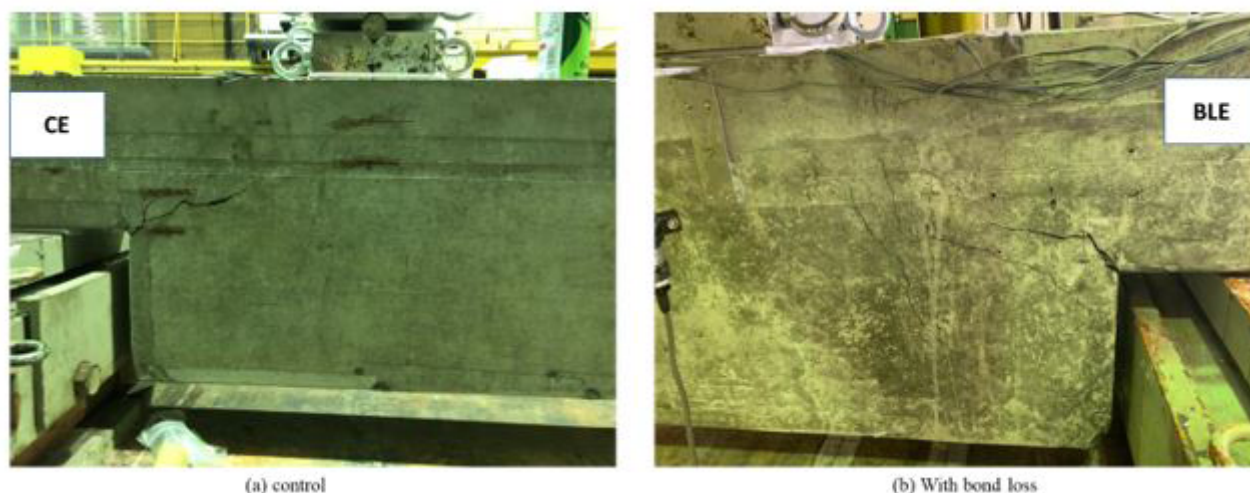
(a) control   (b) With bond loss

FIGURE 18. Failure pattern of RCDEB loaded at a/d=1.5.

FIGURE 19. Failure pattern of RCDEB loaded at the midpoint (17).

started at the reentrant corner and spread towards the compression zone as the monotonic loading increased. Loading at a/d=1.5 resulted in quick failure compared with loading at the midpoint because the hanger reinforcement near the dapped end and the nib longitudinal reinforcement sustained the increasing stresses. However, the tensile reinforcement aided in resisting the crack alongside the hanger reinforcement in the case of loading at the midpoint. In the case of control beams, the diagonal tension cracks formed were relatively between 45° and 60° when measured with a protractor. There was a separation between the bond loss zone at the nib section and the remaining part of the full depth of the RC close to the reentrant portion. The measured crack angle ranged between 25 and 40°. At fairly high stress, diagonal cracks were formed at the full critical depth of the recess portion, resulting in the failure of beams BLE and BEM. This indicates that stresses tend to concentrate at the weak zone under high static loading.

On observing the maximum principal strain of the damage mode of RCDEB under FEM analysis as presented in Figure 20. The loading was gradually applied here at an increment of 5 kN. There is a close conformity between the experiment and the analysis. The crack was initiated at the reentrant corner and propagated with crack width extension. Another diagonal tension

crack formed at the full depth travelled to meet the previous cracks at an incremental loading. In the case of the bond loss specimens BLA and BAM, the reentrant cracks travelled parallel to the longitudinal nib reinforcement indicating the separation of the nib sections from the remaining part of the beam due to the increasing slip action. Flexural cracks culminated in the failure of CAM and BAM when loaded at the midpoint.

As a result of the response under increasing monotonic load, cracking occurs when the induced tensile stress in concrete reaches its ultimate tensile strength near the bond loss region. Due to the loss of tensile stresses in the concrete at the crack position, the stresses in the concrete are subsequently transferred to the reinforcing bars through the bond formed between the concrete and the reinforcement during the cracking stage. Following that, the hanger reinforcement near the recessed corner absorbs additional tensile stresses released by the cracked concrete.

4.3.1. Load versus displacement and strain response of RCDEBs

The cracking load, the failure load and the ductility ratio values for the RCDEBs are itemized in Table 5. Figure 21 shows the load versus displacement relation-
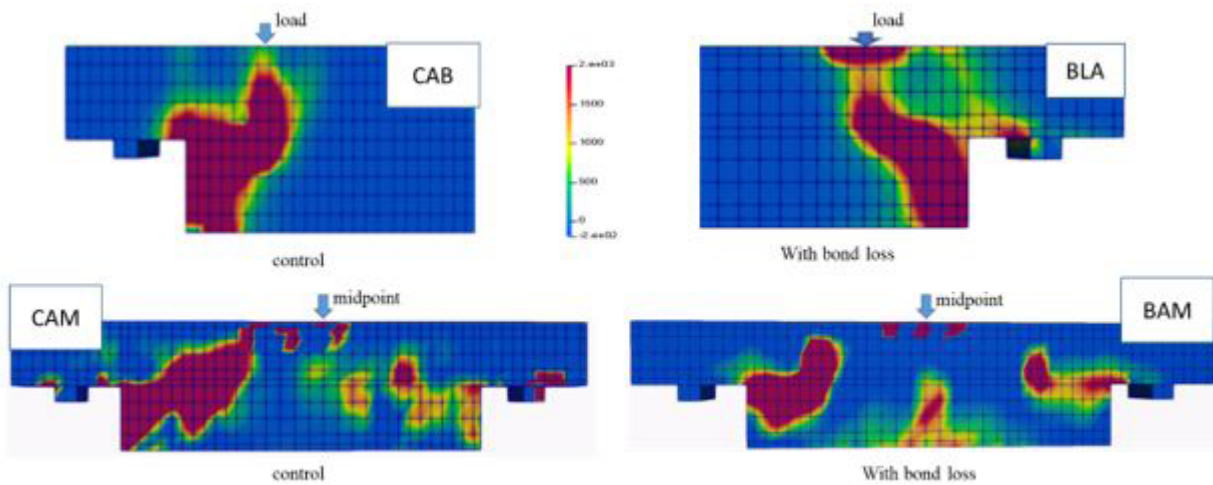
FIGURE 20. Maximum principal strain of damage mode of RCDEB under FEM.

ship between the experiment and analysis comparison of the RCDEBs with and without bond loss influence. The experimental displacement is the net displacement from the beam's supports and the estimated value at the loading point. In comparison, the numerical displacement is determined from the loading point nodes. Figures 22 and 23 present the load versus the strain generated from the hanger reinforcement, the nib longitudinal reinforcement, and the concrete strain close to the active cracks of the beam when subjected to the

loading at a/d of 1.5 and the midpoint, respectively. The strain of the flexural reinforcement on loading at the midpoint is also presented in Figure 23 since the beam experienced concrete cracks at the flexural zone. In the case of the experiment, the strain was obtained automatically using strain gauges connected to the data logger, whereas in the case of the analysis, the space average of the strain localized RC element under the active crack approach was used to obtain the reinforcing bar strains and the concrete strain.
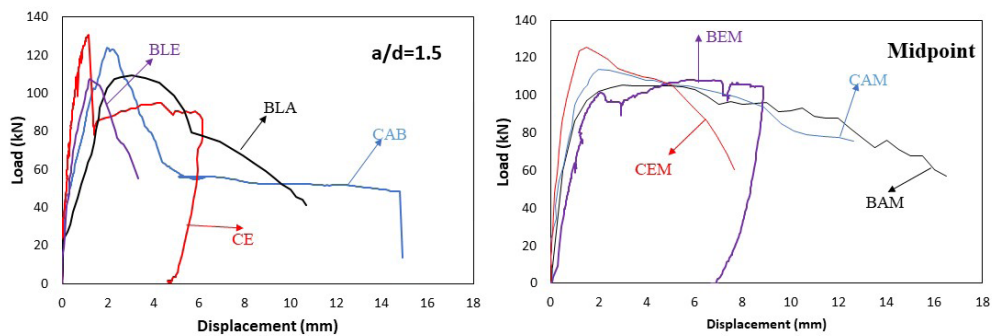

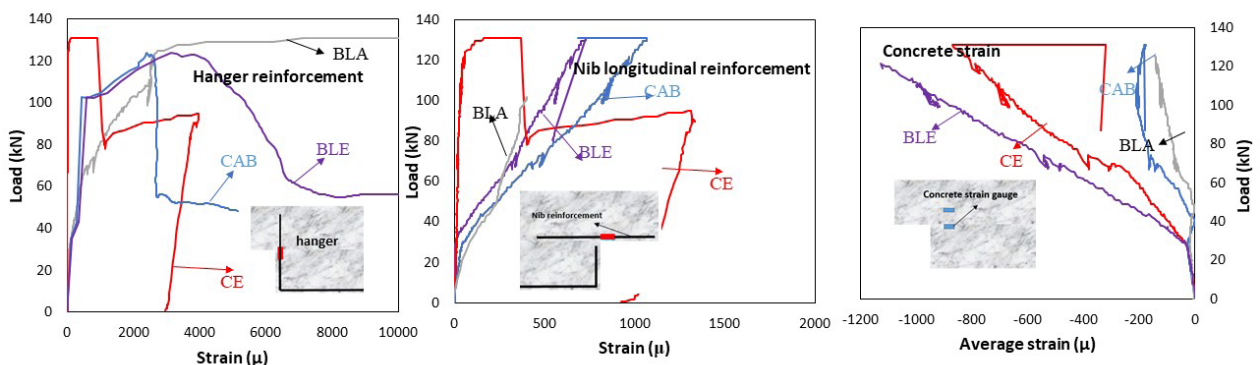**FIGURE 21.** Load versus displacement of RCDEBs for experiment and analysis.

FIGURE 22. Load versus strain response at a/d=1.5 for experiment and analysis.

The experimental control beams (CE and CEM) exhibit significant stiffness up to their full capacity, as shown in Figure 21. When the beams are loaded at a/d of 1.5, the experiment control beam CE has a 6% higher failure load than the analysis control beam CAB and a 21% higher failure load than the experimental bond loss BLE. CAB increases by 10% over the BLA. In the event of midpoint loading, the experiment control CEM has a 10% higher failure load than the analysis control CAM and a 17% higher than BEM. CAM increases by 4% when compared to BAM. Although the analysis shows a considerable increase in ductility over the experiment, the stiffness reduces gradually with increasing monotonic loading due to differences in crack initiation and propagation stage under high tension failure.

The reinforcing bars around the cracks absorbed the rise in tensile stresses when the weak zone developed at the reentrant section due to increased concrete crack width. When loaded at the midpoint and at a/d of 1.5, the hanger reinforcement indicated strain beyond the yield point of 2000μ. However, the nib longitudinal re-

TABLE 5. RCDEBs loading results.

| Specimen RCDEBs	Name	Concrete strength (N/mm²)			Loading and deflection (kN and mm)				
		compressive	splitting	at cracking	δ_y	at failure	Δ_u	Ductility ratio $\left(\Delta_u / \delta_y\right)$
a/d=1.5	CE	42	2.7	105.20	0.2	130.07	1.13	5.65
	BLE	38	2.5	41.48	0.2	107.43	1.20	6.0
	CAB	42	2.7	51.25	0.31	122.80	2.18	7.03
	BLA	38	2.5	31.20	0.38	109.5	3.06	8.05
midpoint	CEM	42	2.7	43.62	0.57	125.56	1.48	2.60
	BEM	38	2.5	38.13	0.57	107.60	6.39	11.21
	CAM	42	2.7	41.60	0.20	114.08	2.75	13.75
	BAM	38	2.5	48.34	0.24	109.34	3.50	14.58
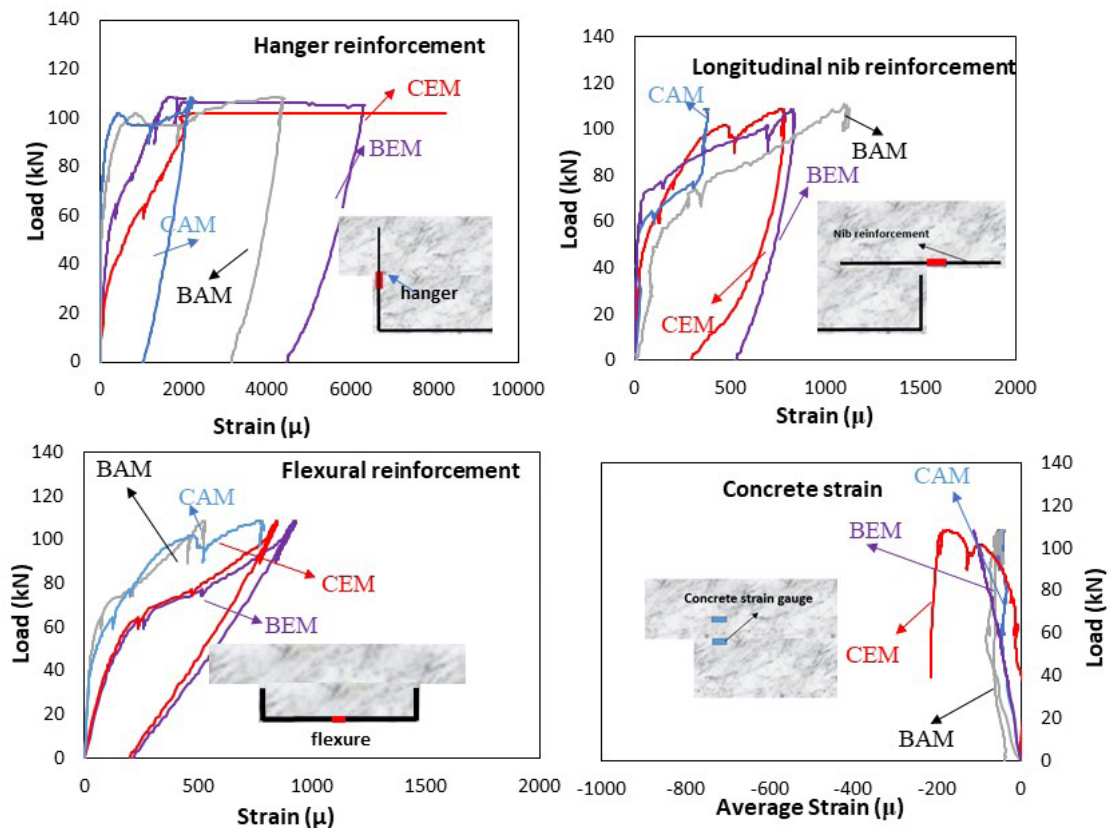
FIGURE 23. Load versus strain response at the midpoint for experiment and analysis.

inforcement did not, as show in Figures 22 and 23. As a result of the significant moment generated by increasing monotonic loading, the hanger reinforcement intersected the cracks, and the strain generated grew dramatically up to the failure load. When the strain of the flexural reinforcement was measured for midpoint loading, the strain value was nearly equal to that of the longitudinal reinforcement, suggesting that the longitudinal reinforcement was sufficient for the nib and tension zone. In the case of concrete strain, the average strain of the strain gauges near the dominant cracks was analyzed, and the concrete strain of 200μ was exceeded in the experiment except for BEM which the stain gauges detached from the concrete substrate. As shown in Figure 23, there was an uneven behaviour in concrete strain in the event of midpoint loading of the analysis beam (CAM and BAM) at the failure load; therefore, a concrete strain value of -200μ could not be determined.

5. CONCLUSIONS

Behaviour of reinforced concrete elements in tension subjected to increasing monotonic loading has been experimentally and numerically evaluated under bond deterioration created in lieu of corrosion between the reinforcing bars and the concrete, the following conclusions are hereby drawn.

1. The present test results on pullout of reinforcing bars from concrete confirms that the bond loss specimens tend to fail in a more brittle, splitting mode, while the control specimens in tend to fail in a less brittle mode. The failure loads were lower than in the control specimen with stiffness loss. The FEM specimens had significantly higher ductility than the experiment due to homogeneity in mesh size, which differed from the experiment's heterogeneous response. No yielding of reinforcement recorded in any specimens.

2. The damage of the RCDEBs was culminated by diagonal tension cracks emerging from the reentrant portion. In the case of the bond loss RCDEB, the nib portion was separated around the reentrant corner from the full depth of the beam under high stress. As a result, the beam suffered immediate damage, resulting in reduced stiffness.

3. After concrete damage, the hanger reinforcement absorbed most of the tensile stresses, resulting in rapid yield strain attainment before failure. The strain was higher when loaded at a/d=1.5 than at the midpoint, demonstrating that the loading was more severe at a lower shear span-to-depth ratio. The nib longitudinal and tensile reinforcements revealed adequate stress resistance without reaching the yield threshold. As a result, the reentrant portion should be strengthened against diagonal tension.

4. Given the current tests' limited scope and range, additional tests covering a broader size range of bars and aggregate are required.

AUTHOR CONTRIBUTIONS:

Conceptualization: A.I. Quadri. Data cleansing: A.I. Quadri. Formal analysis: A.I. Quadri. Research: A.I. Quadri. Methodology: A.I. Quadri. Project administration: A.I. Quadri. Resources: A.I. Quadri. Software: A.I. Quadri. Supervision: A.I. Quadri. Validation: A.I. Quadri. Visualization: A.I. Quadri. Writing-original draft: A.I. Quadri. Writing - review & editing: A.I. Quadri.

REFERENCES

1. Wu, Y.F.; Zhao, X.M. (2013) Unified bond stress–slip model for reinforced concrete. *J. Struct. Eng.* 139 [11], 1951–1962. https://doi.org/10.1061/(ASCE)ST.1943-541X.0000747.

2. Zhao, Y.; Lin, H. (2018) The bond behaviour between concrete and corroded reinforcement: state of the art. University of Leeds, Leeds, West Yorkshire, LS2 9JT, United Kingdom 63–73.

3. Chu, S.H.; Kwan, A.K.H. (2018) A new method for pull out test of reinforcing bars in plain and fibre reinforced concrete. *Eng. Struct.* 164, 82–91. https://doi.org/10.1016/j.engstruct.2018.02.080.

4. Li, X.; Lu, C.; Cui, Y.; Zhou, L. (2023). Study on the bond properties between steel bar and fiber reinforced concrete after high temperatures. *Structures.* 49, 889-902. Retrieved from https://www.sciencedirect.com/science/article/pii/S2352012423001637.

5. Xu, L.; Hai, T.K.; King, L.C. (2014) Bond stress-slip prediction under pullout and dowel action in reinforced concrete joints. *ACI Struct J.* 111 [4], 977-988. https://doi.org/10.14359/51686816.

6. Fang, C.; Lundgren, K.; Chen, L.; Zhu, C. (2004) Corrosion influence on bond in reinforced concrete. *Cem. Concr. Res.* 34 [11], 2159–2167. https://doi.org/10.1016/j.cemconres.2004.04.006.

7. Bamonte, P.F.; Gambarova, P.G. (2007) High-bond bars in nsc and hpc: study on size effect and on the local bond stress-slip law. *J. Struct. Eng.* 133, 225–234. https://doi.org/10.1061/(ASCE)0733-9445(2007)133:2(225).

8. Yukimasa, G. (1971) Cracks formed in concrete around deformed tension bars. *ACI Journal Proceedings.* 68 [4], 244-251. https://doi.org/10.14359/11325.

9. Rossetti, V.A.; Galeota, D.; Giammatteo, M.M. (1995) Local bond stress-slip relationships of glass fibre reinforced plastic bars embedded in concrete. *Mater. Struct.* 28, 340–344. https://doi.org/10.1007/BF02473149.

10. Wu, C.; Chen, G.; Volz, J.S.; Brow, R.K.; Koenigstein, M.L. (2012). Local bond strength of vitreous enamel coated rebar to concrete. *Constr. Build. Mater.* 35, 428-439. https://doi.org/10.1016/j.conbuildmat.2012.04.067.

11. Mousavi, S.S.; Guizani, L.; Ouellet-Plamondon, C.M. (2020) Simplified analytical model for interfacial bond strength of deformed steel rebars embedded in pre-cracked concrete. *J. Struct. Eng.* 146 [8]. https://doi.org/10.1061/(ASCE)ST.1943-541X.0002687.

12. Wang, X.H.; Chen, B.; Tang, P. (2018) Experimental and analytical study on bond strength of normal uncoated and epoxy-coated reinforcing bars. *Constr. Build. Mater.* 189, 612–628. https://doi.org/10.1016/j.conbuildmat.2018.09.010

13. Patel, V.J.; Van, B.C.; Henry, R.S.; Clifton, G.C. (2015) Effect of reinforcing steel bond on the cracking behaviour of lightly reinforced concrete members. *Constr. Build. Mater.* 96, 238–247. https://doi.org/10.1016/j.conbuildmat.2015.08.014.

14. Lutz, L.A.; Gergely, P. (1967) Mechanics of Bond and Slip of Deformed Bars in Concrete. *ACI J. Proceed.* 64 [11], 711-721. https://doi.org/10.14359/7600.

15. Chao, S.; Naaman, A.E.; Parra-Montesinos, G.J. (2009) Bond behavior of reinforcing bars in tensile strain-hardening fiber-reinforced cement composites. *ACI Struct. J.* 106 [6], 897-906. https://doi.org/10.14359/51663191.

16. Quadri, A.I.; Fujiyama, C. (2021) Bond loss response of reinforced concrete dapped-end beam subjected to static and low cycle fatigue loading. *Japan Concr. Inst.* 43, 439–444.

17. Quadri, A.I.; Fujiyama, C. (2021) Response of reinforced concrete dapped-end beams exhibiting bond deterioration subjected to static and cyclic loading. *J. Adv. Concr. Technol.* 19 [5], 536–554. https://doi.org/10.3151/jact.19.536.

18. Tepfers, R.A. (1973) Theory of bond applied to overlapped tensile reinforcement splices for deformed bars. Publ. 73, 2. Department of Concrete Structures, Chalmers University of Technology, Göteborg. 328-345.

19. Somayaji, S.; Shah, S.P. (1981) Bond stress versus slip relationship and cracking response of tension members. *ACI J. Proceed.* 78 [3], 217–225. https://doi.org/10.14359/6920.

20. Mata-Falcón, J.; Pallarés, L.; Miguel, P.F. (2019) Proposal and experimental validation of simplified strut-and-tie models on dapped-end beams. *Eng. Struct.* 183, 594–609. https://doi.org/10.1016/j.engstruct.2019.01.010.

21. Shakir, Q.M. (2020) A review on structural behavior, analysis and design of RC dapped end beams. IOP Conf. Ser. *Mater. Sci. Eng.* 978, 012003. https://doi.org/10.1088/1757-899X/978/1/012003.

22. Taher, S.D. (2005) Strengthening of critically designed girders with dapped ends. Proceedings of the Institution of Civil Engineers. *Struc. Build.* 158 [2], 141–152. https://doi.org/10.1680/stbu.2005.158.2.141.

23. Shakir, Q.M. (2018) Reinforced concrete dapped end beams – state of the art. IJAS 1 [2], 44. https://doi.org/10.30560/ijas.v1n2p44.

24. Shakir, Q.M.; Baneen, B.A. (2020) Retrofitting of self compacting RC half joints with internal deficiencies by CFRP fabrics. *J. Teknol.* 82 [6], 49–62. https://doi.org/10.11113/jurnalteknologi.v82.14416.

25. Mattock, A.H. (2012) Strut-and-tie models for dapped-end beams. *Concr. Inter.* 34-36.

26. Werner, M.P.; Dilger, W.H. (1973) Shear design of prestressed concrete stepped beams. *PCI J.* 18 [4], 37–49. https://doi.org/10.15554/pcij.07011973.37.49.

27. Mattock, A.H.; Chan, T.C. (1979) Design and behavior of dapped-end beams. *PCI J.* 24 [6], 28–45. https://doi.org/10.15554/pcij.11011979.28.45.

28. Aswin, M.; Mohammed, B.S.; Liew, M.S.; Syed, Z.I. (2015) Shear failure of RC dapped-end beams. *Adv. Mater. Sci. Eng.* 2015, 1–11. https://doi.org/10.1155/2015/309135

29. Wang, Q.; Guo, Z.; Hoogenboom, P.C.J. (2005) Experimental investigation on the shear capacity of RC dapped end beams and design recommendations. *Struct. Eng. Mech.* 21 [2], 221–235. https://doi.org/10.12989/SEM.2005.21.2.221.

30. Mohammed, B.S.; Aswin, M.; Liew, M.S.; Zawawi, N. (2019) Structural performance of RC and R-ECC dapped-end beams based on the role of hanger or diagonal reinforcements combined by ECC. *Int. J. Concr. Struct. Mater.* 13, 44. https://doi.org/10.1186/s40069-019-0356-x.

31. Johnson, P. (2007) Report of the commission of inquiryinto the collapse of a portion of the de la Concordeoverpass. The Government of Quebec, Montréal, Canada.

32. di Prisco, M.; Colombo, M.; Martinelli, P.; Coronelli, D. (2018) The technical causes of the collapse of Annone overpass on SS.36. Le cause tecniche del crollo del cavalcavia di Annone. 1–16.

33. Spinella, N.; Messina, D. (2022) Load-bearing capacity of Gerber saddles in existing bridge girders by different levels of numerical analysis. *Struct. Concr.* 24 [1], 211-226. https://doi.org/10.1002/suco.202200279.

34. Fujiyama, C.; Maekawa, K. (2011) A computational simulation for the damage mechanism of steel-concrete composite slabs under high cycle fatigue loads. *J. Adv. Concr. Technol.* 9 [2], 193–204. https://doi.org/10.3151/jact.9.193.

35. Quadri, A.I.; Fujiyama, C. (2021) Numerical analysis of RC Gerber bridge girder subjected to fatigue loading. In: Yokota H, Frangopol DM (eds) Bridge maintenance, safety, management, life-cycle sustainability and innovations, 1st ed. CRC Press, 2682–2689.

36. Quadri, A.I. (2023). Behavior of disturbed region of RC precast beams upgraded with near surface mounted CFRP fiber. *Asian J. Civ. Eng.* 24 [4], 1-15. https://doi.org/10.1007/s42107-023-00605-5.

37. Rakhshanimehr, M.; Esfahani, M.R.; Kianoush, M.R.; Mohammadzadeh, B.A.; Mousavi, S.R. (2014) Flexural ductility of reinforced concrete beams with lap-spliced bars. *Can. J. Civ. Eng.* 41 [7], 594–604. https://doi.org/10.1139/cjce-2013-0074.